JOURNAL OF ADVANCED DIELECTRICS
Vol. 10, No. 3 (2020) 2050009 (7 pages)

DOI: 10.1142/S2010135X20500095

Temperature-dependent energy storage characterization of Pb-free relaxor ferroelectrics

Sarir Uddin*,†,‡,§, Guang-Ping Zheng†, Asif Khan‡, Muhammad Riaz Khan‡ and Banaras Khan‡

*Department of Physics, Government College Hayatabad
Peshawar 25124, Khyber Pakhtunkhwa, Pakistan

†Department of Mechanical Engineering
The Hong Kong Polytechnic University
Hung Hom, Kowloon, Hong Kong

‡Department of Physical and Numerical Sciences
Qurtuba University of Science & Information Technology
Peshawar 25000, Khyber Pakhtunkhwa, Pakistan

§sariruddin@uop.edu.pk

Received 12 January 2020; Revised 20 March 2020; Accepted 14 April 2020; Published 4 July 2020

The energy storage properties of $(1-x)Bi_{0.5}Na_{0.5}TiO_3$–$xBaTiO_3$($0 \le x \le 0.08$) (BNT–BT) ceramics obtained via sol–gel method are determined from the polarization versus electric field (P–E) loops at various temperatures. The energy storage densities are observed to increase with increase in temperature and this may be attributed to the presence of antiferroelectric (AFE) phase at higher temperature ($\ge 120\,^\circ$C). Obvious changes are observed in the saturation polarization (P_s) and remnant polarization (P_r) with increasing temperature. The maximum energy storage density of 0.6 J/cm^3 is observed for $x = 0.06$ in the AFE phase at 150 °C for 90 kV/cm of applied electric field. BNT–BT can be a promising candidate for energy storage devices to be used in above-room-temperature environment.

Keywords: Lead-free; perovskites; relaxor; antiferroelectrics; energy storage.

1. Introduction

Dielectric materials are being used frequently to store electrical energy based on electric polarization by an external applied electric field.[1] Antiferroelectric (AFE) materials possess relatively higher energy storage density (W) compared to the ferroelectric (FE) and the linear dielectric materials.[1,2] The lead (Pb)-based FE and AFE dielectrics, such as lead zirconate (PZ), lead zirconate stannum titanate (PZST) and lead zirconate lanthanum titanate (PZLT), possess relatively better energy storage properties.[2,3] However, due to the hazardous nature of Pb-based compounds, researchers are in search of Pb-free alternatives for capacitors and other electronic devices.[4,5] In this regard, perovskite-structured, Pb-free $Bi_{0.5}Na_{0.5}TiO_3$ (BNT) and its compounds may be better candidates to replace the Pb-based counterparts.[6] Among the BNT-based compounds, $Bi_{0.5}Na_{0.5}TiO_3$–$BaTiO_3$ (BNT–BT) has attracted considerable attention as there exist a morphotropic phase boundary (MPB) and an AFE phase above the room temperature ($T > 120\,^\circ$C).[7–9] BNT–BT exhibits relatively better ferroelectric properties and can be investigated for energy storage properties.[10,11]

The energy storage densities (W) of ferroelectric and antiferroelectric materials can be calculated by[10]

$$W = \int_{P_r}^{P_s} E dp, \tag{1}$$

where E is the external applied electric field, P is the polarization, P_r is the remnant polarization and P_s is the saturation polarization. Equation (1) indicates that W is directly proportional to the electric field and the difference between P_s and P_r. The values of W are calculated by numerical integration of the area in the polarization versus electric field (P–E) loop as shown in Fig. 3.[10–12] The area covered by the P–E curve on the vertical axis gives the recoverable energy storage density.[10–12]

The $(1-x)$BNT–xBT ceramics possess rhombohedral–tetragonal MPB which is reported to be existing in the range of $x = 0.06$–0.1.[13] The AFE phase of BNT–BT is more favorable for relatively higher energy storage applications due to the presence of pinched and double P–E hysteresis loops with higher P_s and lower P_r values.[13,14] In this work,

the energy storage properties of $(1-x)Bi_{0.5}Na_{0.5}TiO_3$–$xBaTiO_3(0\leq x\leq 0.08)$ are explored at various temperatures.

2. Materials and Methods

Solid solutions of $(1-x)Bi_{0.5}Na_{0.5}TiO_3$–$xBaTiO_3$ $(0\leq x\leq 0.08)$ are prepared via the sol–gel method. Solutions of research-grade $Bi(CH3COO)_3$, $Na(CH_3COO)$ and $Ba(CH_3COO)_2$ in stoichiometric ratios are separately prepared in acetic acid on a hot plate with a magnetic stirrer at 60°C. The solution of $C_{16}H_{36}O_4Ti$ is prepared in ethanol to which acetyl acetone is added drop-wise for stabilization. All four solutions are mixed in a flask on a hot plate with stirrer. A dark yellow colored gel is obtained by heating the stock solution at 80 °C for 4 h on a hot plate. The gel is dried on a hot plate at 100 °C and calcined in air at 800 °C for 2 h with 5 °C/min heating and cooling rates. For each sample, two drops of polyvinyl alcohol (PVA) are added and mixed with calcined powders as a binder and then this mixture is pressed by uniaxial presser at 100 MPa in disk shapes of 15-mm diameter. The pellets are sintered at 1200 °C for 2 h with 5 °C/min heating and cooling rates in air.

The phase analyses of fabricated samples are carried out via X-ray diffractometer (XRD; Bruker D8 Advance) using cobalt-K_α radiation ($\lambda = 0.17902$ nm). The microstructural analyses are carried out via scanning electron microscopy (SEM). The temperature-dependent relative permittivity (ε_r) and loss tangent ($\tan\delta$) of ceramics are measured at different frequencies using impedance analyzer (HP4192A). The temperature-dependent *P*–*E* hysteresis loops are obtained by temperature-controlled TF Analyzer at a frequency of 10 Hz. The energy storage properties at selected temperatures are calculated using Eq. (1) and utilizing the *P*–*E* hysteresis loops.

3. Results and Discussion

3.1. *Phase and microstructural analyses*

The room-temperature XRD patterns of $(1-x)Bi_{0.5}Na_{0.5}TiO_3$–$xBaTiO_3(0\leq x\leq 0.08)$ ceramics [Fig. 1(a)] revealed the formation of single-phase perovskite-structured compositions. The (110) peaks are shifted to relatively lower 2θ values with increasing BT content [Fig. 1(b)]. This shift may be attributed to the incorporation of relatively larger Ba^{+2} ($R_{Ba} = 1.61$ Å) ions for smaller Bi^{+3}/Na^{+} ($R_{Bi}/R_{Na} =$ 1.40 Å/1.39 Å) ions on the *A*-site of the perovskite unit cell.[15] The emergence of an obvious (002) shoulder peak at 53.5° along with (200) peak for x=0.08 indicated the coexistence of the rhombohedral (*R*3*m*) and tetragonal (*P*4 mm) phases, consistent with previous studies which reported the existence of MPB at $0.05\leq x\leq 0.1$ in $(1-x)$BNT–xBT ceramics.[13,16]

The secondary-electron SEM images of BNT–BT ceramic samples calcined at 800 °C and sintered at 1200 °C for 2 h in air are shown in Fig. 2. The pellets are polished and thermally etched at 1000 °C for 20 min. The grain morphologies are observed to change from rough-edged spheroidal shape to relatively sharp-edged cuboidal shape with increasing BT content. The grains in each sample are nearly of uniform size ($\sim 1\times 1\,\mu m^2$) for $0\leq x\leq 0.08$. Some slightly elongated ($\sim 1\times 1.2\,\mu m^2$) grains are also observed. Previous studies on BNT–BT ceramics reported a decrease in grain size with increasing BT content.[11,16]

3.2. *Phase transition analysis*

The phase transition phenomenon with increasing temperature in the fabricated $(1-x)Bi_{0.5}Na_{0.5}TiO_3$–$xBaTiO_3$ $(0\leq x\leq 0.08)$ ceramic samples is indirectly investigated via temperature-dependent dielectric properties as shown in Fig. 3.

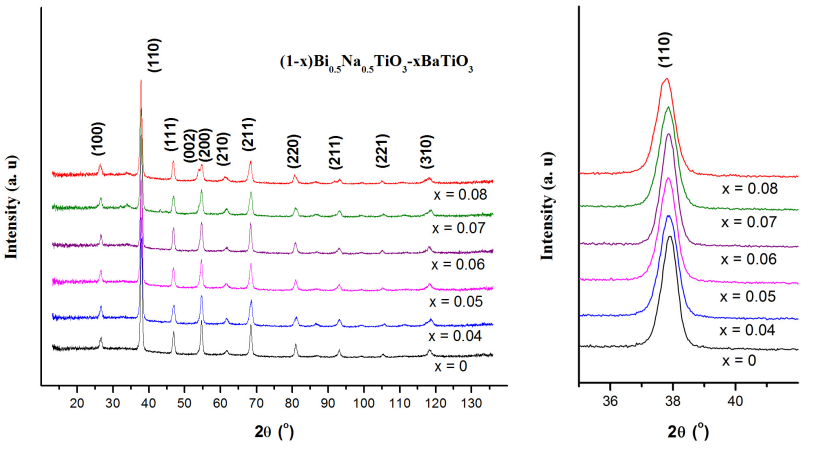

Fig. 1. (a) The XRD patterns of $(1-x)Bi_{0.5}Na_{0.5}TiO_3$–$xBaTiO_3(0\leq x\leq 0.08)$ ceramics indicating single-phase perovskite-structured compositions. (b) The (110) peaks being shifted to lower 2θ values.

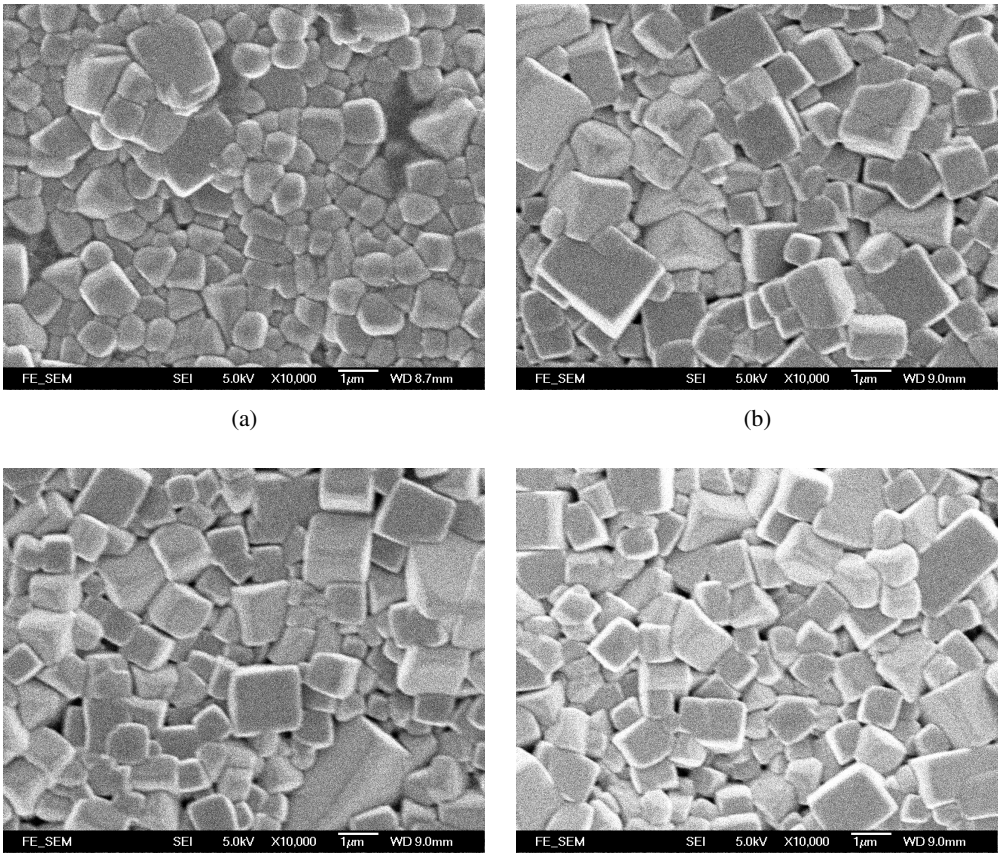

(a) (b) (c) (d)

Fig. 2. Secondary-electron SEM images of selected $(1-x)Bi_{0.5}Na_{0.5}TiO_3$–$xBaTiO_3$ ceramic samples for (a) $x = 0$, (b) $x = 0.04$, (c) $x = 0.06$ and (d) $x = 0.08$.

The values of the dielectric constant (ε_r) and dielectric loss $(\tan\delta)$ are plotted versus temperature (T) at different frequencies. Two anomalies are observed on ε_r versus T curves at temperatures denoted by T_d and T_m corresponding to the depolarization and maximum dielectric constant, respectively. The first anomaly observed at around 120 °C may be attributed to the FE–AFE phase transition consistent with the $\tan\delta$ versus T curve showing an anomaly at the same temperature. The second anomaly observed at T_m (250 °C–320 °C) may be attributed to the AFE–paraelectric (PE) phase transition associated with the Curie point (T_c).[7–9] The broadness of all the relative permittivity curves along with a frequency dispersion obvious at T_m demonstrates the relaxor behavior of $(1-x)$BNT–xBT ceramics and somewhat diffuse

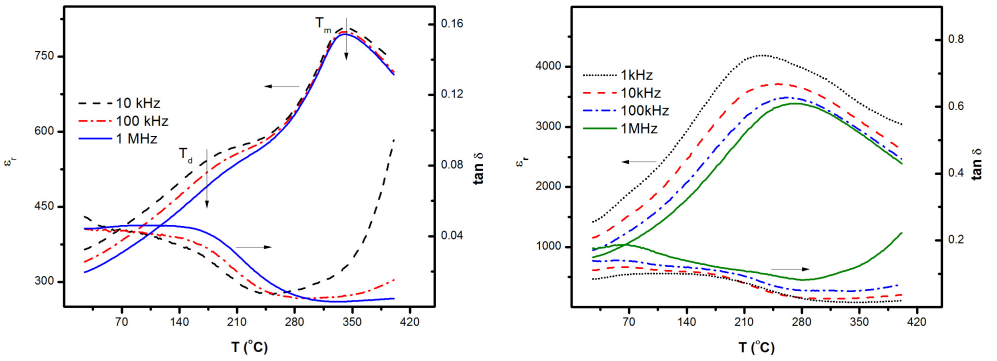

(a) (b)

Fig. 3. Plots of ε_r and $\tan\delta$ versus T of $(1-x)Bi_{0.5}Na_{0.5}TiO_3$–$xBaTiO_3$ ceramics for (a) $x = 0$, (b) $x = 0.04$, (c) $x = 0.06$ and (d) $x = 0.08$, showing the FE–AFE and AFE–PE phase transitions.

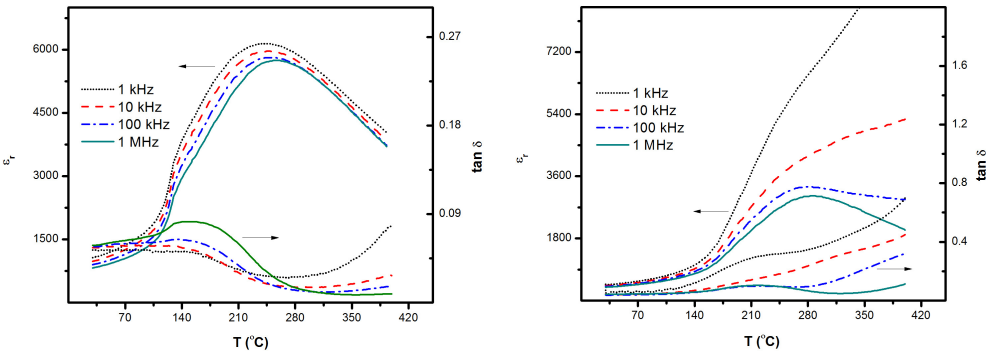

Fig. 3. (*Continued*)

phase transition from FE to AFE phase and then to a centrosymmetric cubic PE phase.[17,18] T_m is observed to decrease from 320 °C to 250 °C with an increase in BT content. The dielectric constant (ε_r) increases with increase in BT content specifically around T_m which may be attributed to the substitution of relatively larger ions of Ba^{2+} for Bi^{3+} and Na^{+} at *A*-site of the perovskite unit cell.[15] The observed increase in $\tan\delta$ at higher temperatures ($> 210°C$) may be due to increase in conductivity of samples caused by thermal excitation.[9]

3.3. *Ferroelectric properties*

The polarization versus electric field (*P*–*E*) hysteresis loops of $(1-x)$BNT–*x*BT ceramics at various temperatures are shown in Fig. 4. All plots indicated similar trend of a rise in

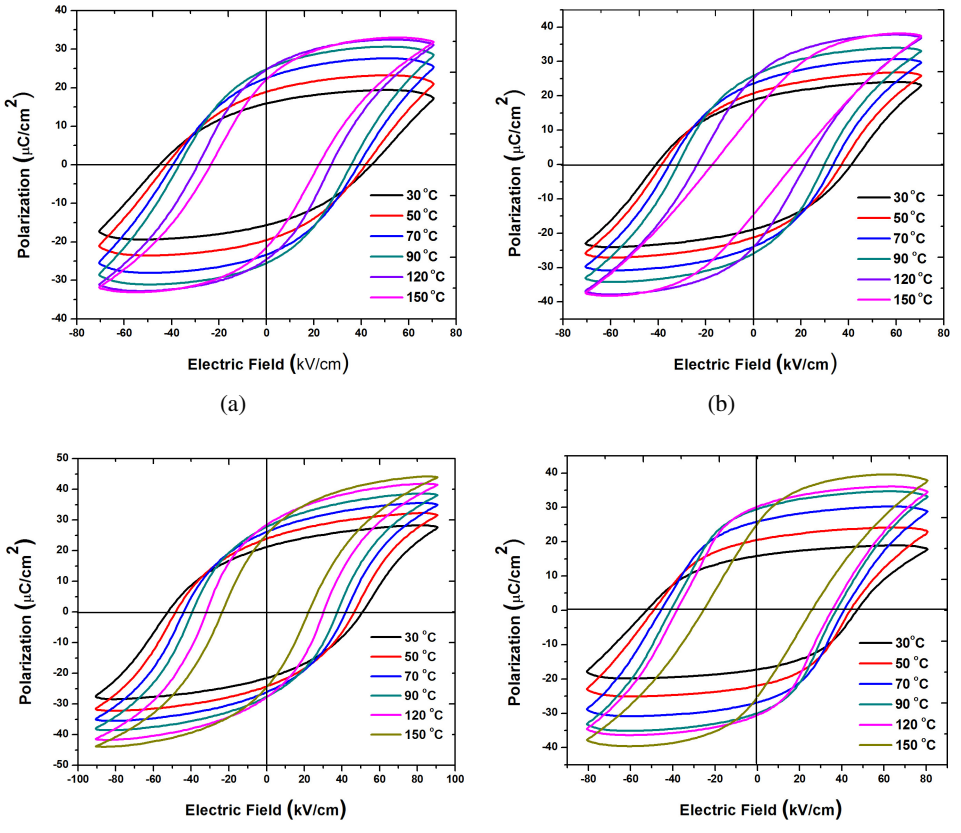

Fig. 4. Temperature-dependent *P*–*E* loops of selected $(1-x)$BNT–*x*BT ceramic samples at different temperatures for (a) $x = 0.04$, (b) $x = 0.05$, (c) $x = 0.06$ and (d) $x = 0.08$.

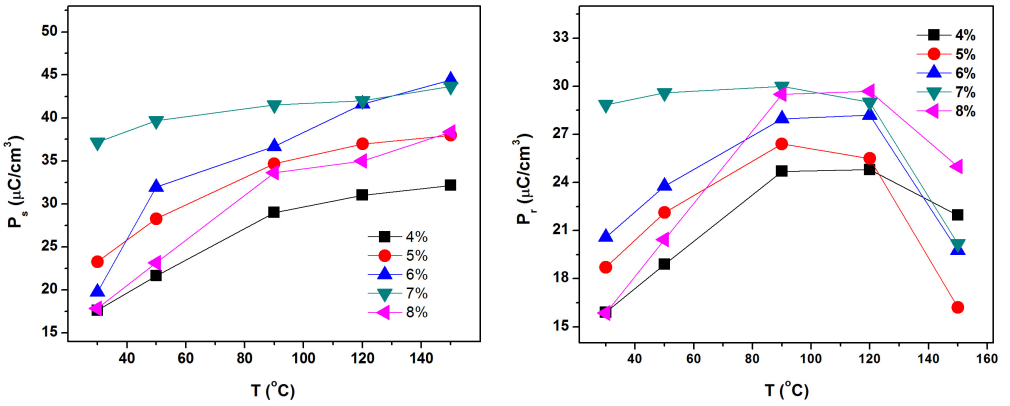

(a) (b)

Fig. 5. Plots of (a) saturation polarization (P_s) versus temperature and (b) remnant polarization (P_r) versus temperature for different BT contents.

P_r in the FE phase ($T < 120\,^{\circ}$C) and a fall gradually in the AFE phase ($T > 120\,^{\circ}$C) as summarized in Fig. 5. The temperature-dependent values of P_s obtained for BNT–BT [Fig. 5(a)] in this study are found consistent with a previous work.[19] Thermal excitation with increase in temperature below T_d ($T < 120\,^{\circ}$C) may align some antiparallel dipoles with the electric field and hence causes an increase in P_s.[19] Samples with high BT contents are found to have relatively higher dielectric strength and possess relatively larger P_s values. It is observed that P_s increases with increase in T while P_r increased at temperatures below T_d and decreased for those above T_d (Figs. 4 and 5). The values of coercive electric field (E_c) decreased with increasing the temperature which is consistent with previous studies on BNT–BT.[19,20] The P–E hysteresis loops deform with the increase in temperature and pinched loops start appearing at about 120 °C for the BNT–BT ceramics (Fig. 4). Pinched and thin P–E hysteresis loops indicate the presence of AFE phase above T_d in the BNT–BT compositions.[21]

3.4. *Energy storage properties*

The energy storage densities (W) of $(1-x)Bi_{0.5}Na_{0.5}TiO_3$–$x$ $BaTiO_3$($0 \le x \le 0.08$) samples are calculated using Eq. (1) from the P–E loops for different BT contents at various values of temperature. The maximum value of W obtained is 0.6 J/cm^3 at 150° C for $x = 0.06$ under 90 kV/cm^3 of applied electric field. Our obtained results for W are comparable with the previously reported value of 0.485 J/cm^3 for BNT–BT at room temperature, synthesized via solid-state route.[22] Recently, Li *et al.*[23] reported an energy storage density of 1.2 J/cm^3 for 15% $BaSnO_3$-doped 0.94BNT–0.06BT at 115 kV/cm. The value of energy storage density of BNT–BT [Fig. 6(a)] increases from 0.18 J/cm^3 to 0.6 J/cm^3 with the increase in BT contents from 0.04 to 0.06. However, for $x = 0.08$, W decreased slightly which may be attributed to the increase in dielectric loss as indicated in Fig. 3(d).[24] Figure 6(b) indicates that energy density of BNT–BT samples increases monotonically with the increase in temperature from 30 °C to 150 °C for all compositions. The increase in W

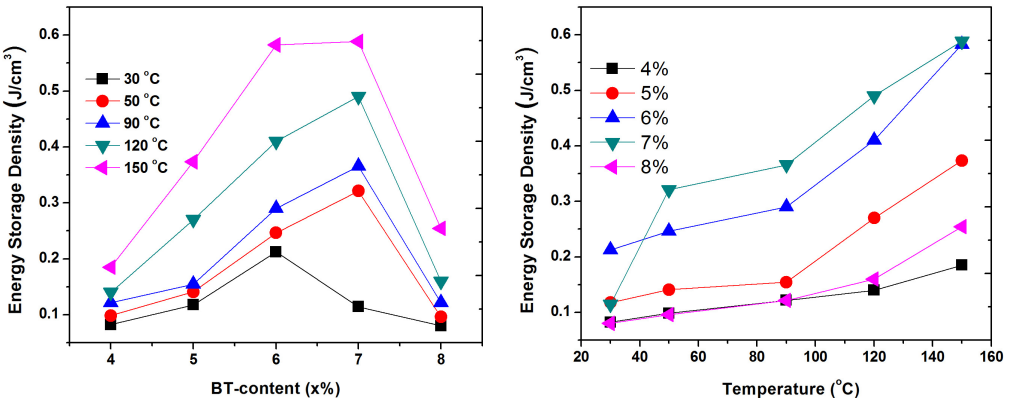

(a) (b)

Fig. 6. Energy storage properties of $(1-x)$BNT–xBT: (a) Energy storage density (W) versus BT content at various temperatures and (b) W versus T for different BT contents.

with increase in temperature may be attributed to the phase transformation from FE to AFE phase above 100 °C.[8,16,20]

In order to obtain higher values of W, two parameters need to be higher, namely the electric polarization produced and the applied external electric field.[10] The electric polarization is an intrinsic property of a material related to the crystal symmetry while the maximum electric field that a material can withstand depends on its dielectric strength. Higher value of electric field in units of kV/cm can be achieved by utilizing thin films of dielectrics as obtained (12.4 J/cm^3) by Zhao *et al.*[25] for modified BNT at 1200 kV/cm. The energy storage density can be enhanced if multilayered thin films of dielectrics are utilized in the capacitors.[26] Hence, as a whole it can be concluded that BNT–BT may be utilized in capacitors to be used effectively in relatively higher temperature environment.

4. Conclusions

Ceramic compounds of $(1-x)Bi_{0.5}Na_{0.5}TiO_3$–$xBaTiO_3$ ($0 \leq x \leq 0.08$) were fabricated via the chemical sol–gel method. The temperature-dependent dielectric values revealed two phase transitions in the samples. The P_s value increased monotonically with the increase in temperature while the P_r value increased with the increase in temperature below T_d and decreased above T_d. The decrease of P_r above T_d may be attributed to the presence of AFE phase above T_d. The maximum energy storage density of 0.6 J/cm^3 at 150 °C was observed for 0.94BNT–0.06BT compound for 90 kV/cm of applied electric field. BNT–BT fabricated via the sol–gel method can be a better candidate for the energy storage applications at higher temperature.

Acknowledgments

This work was supported by the Foshan Xianhu Laboratory of the Advanced Energy Science and Technology Guangdong Laboratory, China. The authors also acknowledge the financial support extended by the technology Innovation Commission of Shenzhen, China and the Higher Education Commission (HEC), Pakistan.

References

[1]Z. Hao, A review on the dielectric materials for high energy-storage application, *J. Adv. Dielect.* **3**, 1330001 (2013).
[2]M. S. Mirshekarloo, K. Yao and T. Sritharan, Large strain and high energy storage density in orthorhombic perovskite $(Pb_{0.97}La_{0.02})(Zr_{1-x-y}Sn_xTi_y)O_3$ antiferroelectric thin films, *Appl. Phys. Lett.* **97**, 142902 (2010).
[3]X. F. Chen, X. L. Dong, G. S. Wang, F. Cao and Y. L. Wang, Doped Pb(Zr,Sn,Ti)O_3 slim-loop ferroelectric ceramics for high-power pulse capacitors application, *Ferroelectrics* **363**, 56 (2008).
[4]J. Rödel, W. Jo, K. T. P. Seifert, E.-M. Anton, T. Granzow and D. Damjanovic, Perspective on the development of lead-free piezoceramics, *J. Am. Ceram. Soc.* **92**, 1153 (2009).
[5]Y. Zhang, M. Cao, Z. Yao, Z. Wang, Z. Song, A. Ullah, H. Hao and H. Liu, Effects of silica coating on the microstructures and energy storage properties of $BaTiO_3$ ceramics, *Mater. Res. Bull.* **67**, 70 (2015).
[6]W.-S. Kang and J.-H. Koh, $(1-x)Bi_{0.5}Na_{0.5}TiO_3$–$xBaTiO_3$ lead-free piezoelectric ceramics for energy-harvesting applications, *J. Eur. Ceram. Soc.* **35**, 2057 (2015).
[7]M. Cernea, E. Andronescu, R. Radu, F. Fochi and C. Galassi, Sol-gel synthesis and characterization of $BaTiO_3$-doped $(Bi_{0.5}Na_{0.5})TiO_3$ piezoelectric ceramics, *J. Alloys Compd.* **490**, 690 (2010).
[8]W. Jo, J. E. Daniels, J. L. Jones, X. Tan, P. A. Thomas, D. Damjanovic and J. Rödel, Evolving morphotropic phase boundary in lead-free $(Bi_{1/2}Na_{1/2})$ TiO_3–$BaTiO_3$ piezoceramics, *J. Appl. Phys.* **109**, 014110 (2011).
[9]X. Tan, E. Aulbach, W. Jo, T. Granzow, J. Kling, M. Marsilius, H.-J. Kleebe and J. Rödel, Effect of uniaxial stress on ferroelectric behavior of $(Bi_{1/2}Na_{1/2})TiO_3$-based lead-free piezoelectric ceramics, *J. Appl. Phys.* **106**, 044107 (2009).
[10]C.-S. Chen, C. S. Tu, P.-Y. Chen, Y. Ting, S.-J. Chiu, C. Hung, H.-Y. Lee, S.-F. Wang, J. Anthoninappen, V. H. Schmidt and R. R. Chien, Dielectric properties in lead-free piezoelectric $(Bi_{0.5}Na_{0.5})TiO_3$–$BaTiO_3$ single crystals and ceramics, *J. Cryst. Growth* **393**, 129 (2014).
[11]A. Chaouchi, S. Kennour, S. d'Astorg, M. Rguiti, C. Courtois, S. Marinel and M. Aliouat, Characterization of sol–gel synthesised lead-free $(1-x)Na_{0.5}Bi_{0.5}TiO_3$–$xBaTiO_3$-based ceramics, *J. Alloys Compd.* **509**, 9138 (2011).
[12]M. Liu, H. Zhu, Y. Zhang, C. Xue and J. Ouyang, Energy storage characteristics of $BiFeO_3$/$BaTiO_3$ Bi-layers integrated on Si, *Materials* **9**, 935 (2016).
[13]P. Chen, J. Wang, W. Zeng, C. Zhou, Y. Zhang, Q. Li, J. Xu, G. Chen and C. Yuan, Dielectric behaviors and relaxor characteristics in $Bi_{0.5}Na_{0.5}TiO_3-BaTiO_3$ ceramics, *J. Adv. Dielect.* **9**, 1950038 (2019).
[14]T. Oh and M.-H. Kim, Phase relation and dielectric properties in $(Bi_{1/2}Na_{1/2})_{1-x}Ba_xTiO_3$ TiO_3 lead-free ceramics, *Mater. Sci. Eng. B* **132**, 239 (2006).
[15]R. D. Shannon, Revised effective ionic radii and systematic studies of interatomic distances in halides and chalcogenides, *Acta Crystallogr. A* **32**, 751 (1976).
[16]Y. S. Sung, J. M. Kim, J. H. Cho, T. K. Song, M. H. Kim and T. G. Park, notRoles of lattice distortion in $(1-x)(Bi_{0.5}Na_{0.5})$ $TiO_{3-x}BaTiO_3$ ceramics, *Appl. Phys. Lett.* **96**, 202901 (2010).
[17]W. Jo, S. Schaab, E. Sapper, L. A. Schmitt, H.-J. Kleebe, A. J. Bell and J. Rödel, On the phase identity and its thermal evolution of lead free $(Bi_{1/2}Na_{1/2})TiO_3$–6 mol% $BaTiO_3$, *J. Appl. Phys.* **110**, 074106 (2011).
[18]W. Ge, H. Cao, C. DeVreugd, J. Li, D. Viehland, Q. Zhang and H. Luo, Influence of $BaTiO_3$ content on the structure and properties of $Na_{0.5}Bi_{0.5}TiO_3$ crystals, *J. Am. Ceram. Soc.* **94**, 3084 (2011).
[19]Y. Bai, G.-P. Zheng and S.-Q. Shi, Abnormal electrocaloric effect of $Na_{0.5}Bi_{0.5}TiO_3$–$BaTiO_3$ lead-free ferroelectric ceramics above room temperature, *Mater. Res. Bull.* **46**, 1866 (2011).
[20]S. T. Zhang, A. B. Kounga, E. Aulbach and Y. Deng, Temperature-dependent electrical properties of $0.94Bi_{0.5}Na_{0.5}TiO_3$–$0.06BaTiO_3$ ceramics, *J. Am. Ceram. Soc.* **91**, 3950 (2008).
[21]A. Pathak, R. Chatterjee and C. Prakash, Improvement in shape memory in magnesium niobate modified PZST, *Ceram. Int.* **36**, 2263 (2010).

[22]M. Chandrasekhar and P. Kumar, Synthesis and characterizations of BNT-BT and BNT-BT-KNN ceramics for actuator and energy storage applications, *Ceram. Int.* **41**, 5574 (2015).
[23]Q. Li, M. Li, C. Wang, M. Zhang and H. Fan, Enhanced temperature stable dielectric properties and energy-storage density of $BaSnO_3$-modified $(Bi_{0.5}Na_{0.5})_{0.94}Ba_{0.06}TiO_3$ lead-free ceramics, *Ceram. Int.* **45**, 19822 (2019).
[24]M. Rawat and K. L. Yadav, Structural, dielectric and ferroelectric properties of $Ba_{1-x}(Bi_{0.5}Na_{0.5})_xTiO_3$ ceramics, *Ceram. Int.* **39**, 3627 (2013).
[25]Y. Zhao, X. Hao and M. Li, Dielectric properties and energy-storage performance of $(Na_{0.5}Bi_{0.5})TiO_3$ thick films, *J. Alloys Compd.* **601**, 112 (2014).
[26]Y. Bai, G. P. Zheng and S. Q. Shi, Kinetic electrocalorific effect and giant net cooling of lead-free ferroelectric refrigerants, *J. Appl. Phys.* **108**, 104102 (2010).